

Full Length Article

Thermal conductivity of TPMS lattice structures manufactured via laser powder bed fusion

S. Catchpole-Smith^a, R.R.J. Sélo^a, A.W. Davis^d, I.A. Ashcroft^a, C.J. Tuck^a, A. Clare^{b,c,*}^a Additive Manufacturing & 3D Printing Research Group, The University of Nottingham, Nottingham, NG7 2RD, UK^b Advanced Manufacturing Group, Faculty of Engineering, The University of Nottingham, Nottingham, NG7 2RD, UK^c Department of Mechanical, Materials and Manufacturing Engineering, Faculty of Science and Engineering, University of Nottingham China, 199 Taikang East Road, University Park, Ningbo, 315100, China^d Siemens Industrial Turbomachinery Ltd, Waterside South, Lincoln, Lincolnshire, LN5 7FD, UK

ARTICLE INFO

Keywords:

Laser powder bed fusion
Additive manufacture
Thermal conductivity
Heat transfer
Nickel
Titanium
Lattice structure
TPMS

ABSTRACT

Lattice structures can add value to high-performance components manufactured by laser powder bed fusion due to their high specific strength and stiffness. A further use of lattice structures is in thermo-mechanical applications, where the high surface area of the lattice may aid heat transfer. However, little characterisation of lattices under thermal loading is currently available in the literature. In this study, a custom-built test rig was used to characterise the thermal conduction for three triply periodic minimal surface lattice types, namely: gyroid, diamond and Schwarz primitives, with unit cell size and volume fraction being varied.

Results show that thermal conductivity is primarily a function of the material properties and volume fraction of the sample. However, some effects of the geometry, such as surface area to volume ratio, can be used to explain slight differences in the measured conductivity. The Schwarz primitive unit cell consistently gave the highest conductivity, with diamond and gyroid unit cells being marginally lower. Larger cell sizes typically gave higher conductivity than smaller cells, which can be attributed to greater intra-cell convective heat transfer and better interface coupling with the testing apparatus.

The experimental results are used to derive equations that allow samples with a specified thermal conductivity to be designed, thus demonstrating how a component may be manufactured with a custom thermal profile by varying the volume fraction of the lattice.

1. Introduction

Additive manufacturing (AM) has the potential to drastically change the way components for heat transfer are designed and manufactured. Components operating at elevated temperatures require efficient dissipation of thermal energy to prevent failure. Whilst the demands on cooling systems are increasing in the pursuit of component performance gains, the package size available for heatsinks and ancillaries is decreasing. Laser powder bed fusion (LPBF) enables the manufacture of components without the need for tooling [1]. Hence, complex geometries, such as cellular structures, can be manufactured that are not otherwise possible using conventional processes. Cellular structures underpin some of the most efficient solutions to engineering problems faced in nature [2], such as strong but flexible trabecular bone and routes for fluid transport in plants. Importantly, they can provide a range of heat transfer augmentation including high heat exchange, heat shielding or insulation, and flame arresting [3]. One family of cellular

structures is triply-periodic minimal surface (TPMS) lattice structures, mathematically derived unit-cells that can be repeated in 3-dimensions to form lightweight, high-strength structures [4]. These structures can provide the high surface-area-to-volume ratio required for effective convective heat transfer, the performance of which will be explored in forthcoming work. AM has the potential to enable highly efficient cooling designs that provide excellent heat transfer per unit volume or unit mass. However, only limited investigations into AM of lattice structures for heat transfer have been undertaken to date.

Historically, heatsink geometry has been varied to optimise the balance between heat transfer performance and mass. However, heat transfer geometries are heavily constrained by conventional manufacturing methods such as sheet forming, extrusion [5], welding [6] or investment casting. This is especially true for components with internal cooling features such as turbine blades, where complex cooling channels may provide the greatest benefit but simply cannot be implemented effectively via conventional investment casting manufacture. Combining

* Corresponding author.

E-mail address: adam.clare@nottingham.ac.uk (A. Clare).

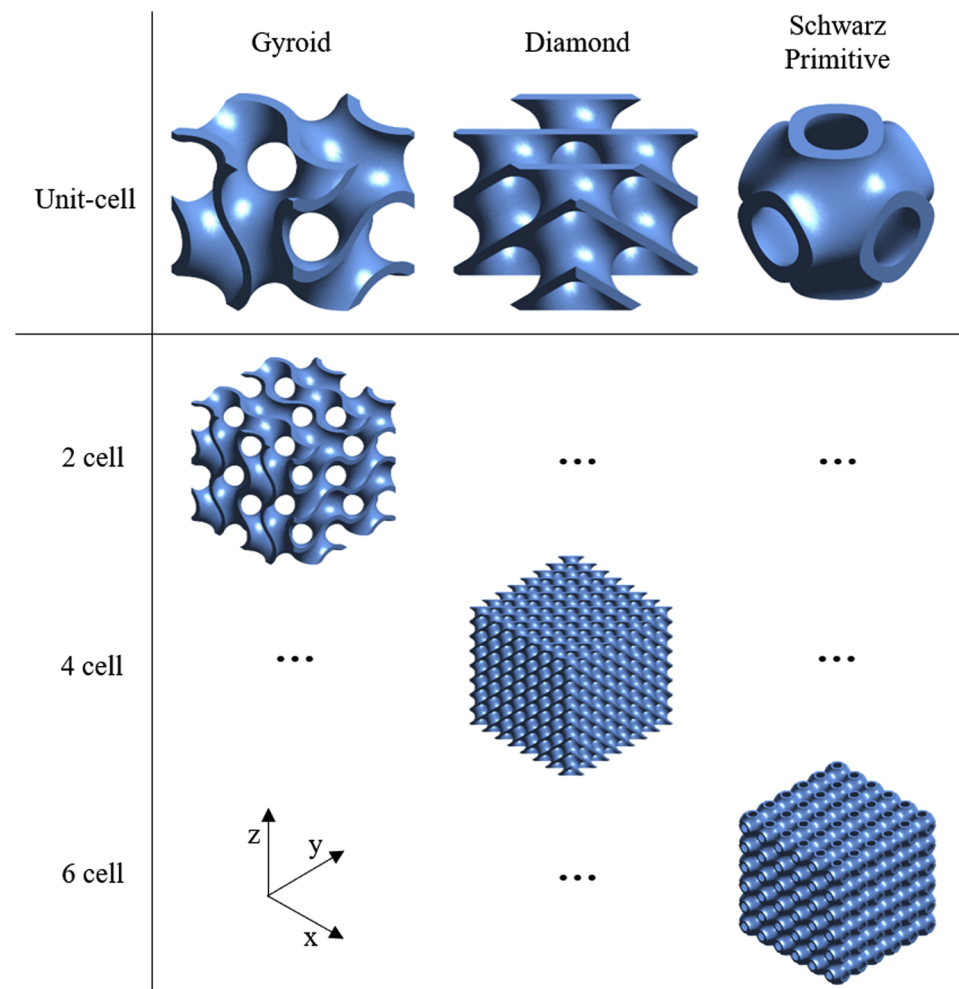


Fig. 1. Single unit-cell models with lattice dimensions [1,1,1] for each of the three unit-cell types used in this study.

this requirement with the need to reduce the mass of turbine engines for increased fuel efficiency, TPMS lattice structures with good thermo-mechanical performance have the potential to replace the pin-fins [7,8], honeycombs [9,10] and sandwich panels [11,12] that are traditionally employed in heat transfer applications. Introduction of lattice structures for thermomechanical applications in the gas turbine hot section will likely begin with static components due to the low degree of mechanical loading in comparison to rotating components. Until confidence is gained in qualification of LPBF manufactured lattice structures, their use in the most critical applications will be limited.

LPBF has been widely used to manufacture a range of strut-type lattices, characterised by a node and element topology, where the elements are typically constant cross-section struts. Such examples are the body-centred cubic (BCC) unit cell [13] and the BCC-Z unit cell [14]. However, such LPBF manufactured lattices have not been characterised for use in heat transfer applications. This is despite conventionally manufactured samples of similar geometry being shown to perform well in convective heat transfer [15], with the potential for bi-functionality when used in combined thermal and mechanical loading [16]. The use of lattice structures in thermo-mechanical applications was identified by Gu et al. [17], who demonstrated that continuous cross-section (2D) lattice sandwich panels can be optimised for combined thermal and mechanical performance. It was shown that optimisation favoured either structural stiffness or thermal performance; both factors could not be optimised concurrently due to the geometry of the chosen strut-type lattices. The triangular geometry that provided the highest stiffness had lower thermal performance than the other geometries and the honeycomb structure with the best thermal performance had reduced

mechanical strength in comparison to the triangular geometry. TPMS lattice structures have the potential to improve upon these results by providing the high specific stiffness required to meet targets for mass reduction alongside enhanced thermal performance over strut-type lattice structures.

Wong et al. [18] used LPBF to manufacture pin-fin heat exchanger designs in stainless steel (316 L) and aluminium (6061). The geometries included circular and diamond cross-sections, with an additional lattice type structure consisting of elliptical cross-sections built at an angle to the substrate. This study was extended in subsequent work with a strut-type lattice that was said to be modelled on the geometries typically used as support structures in LPBF [19]. Whilst the lattice structures chosen by Wong et al. significantly increased the surface area to volume ratio, typically the driver for effective convective heat transfer, the struts were too thin to provide sufficient thermal conductivity. This resulted in a large temperature gradient along the strut length, reducing the effective fin efficiency. Further, the fluid flow had poor interaction with the geometry of the lattice due to alignment of features in the fluid flow direction; struts downstream of the air flow are in the low-velocity wake produced by upstream struts, reducing the heat transfer. With TPMS lattices, both of these failures may be addressed. Dependent on the application, unit cells can be chosen that force the coolant fluid to frequently change direction or divert around a feature, resulting in increased fluid interaction with the structure. Further, thick wall sections that are a feature of some TPMS structures can join hot-side to cold-side to provide a high thermal conductivity path to draw heat away from a source. Volume fraction grading can be utilised to provide this increased conductivity where it is required but keep mass to a

minimum by removing material in cooler regions of the structure.

To fully understand the thermal performance of different lattices, the modes of heat transfer, conduction and convection, must be analysed. This study acts as a standalone source for performance in thermal conduction applications. The performance of TPMS lattice structures under conduction heat transfer is experimentally determined using a custom-built testing apparatus conforming to ASTM E1225-13. The data presented here can help to enable the use of TPMS lattice structures in basic thermo-mechanical applications, for example, in a component that requires a specified thermal insulation between two surfaces, but needs to retain a high degree of mechanical strength. Further, this determination of thermal conductivity characteristics acts as a precursor to fully understanding the performance of TPMS lattice structures convective heat transfer.

2. Experimental method

2.1. Unit cell types

Three different TPMS unit-cell types were investigated in this study: gyroid, diamond and Schwarz primitive. The lattice models were generated using in-house software, 'FLatt Pack', and output as .stl files. A single unit-cell is described as having a cell number of 1; this corresponds to an array of [1,1,1] unit-cells in the direction [x, y, z], as illustrated in Fig. 1.

2.2. Geometric experimental parameters

A total of 18 lattice samples were manufactured over three unit-cell types as shown in Table 1. Sample dimensions are $20 \times 20 \times 20$ mm with cell numbers of 2, 4 and 6, where a cell number of 4 corresponds to a [4,4,4] unit-cell array using the notation described in Fig. 1. Due to the fixed sample dimensions, this equates to cell sizes of 10, 5 and 3.3 mm respectively to achieve a cube with side lengths of 20 mm. It is important to understand any effects that size scale may have on the thermal conductivity performance of lattice structures. Therefore, this range of unit cell sizes is chosen to cover different potential component size scales – 10 mm cells may be used in components with void thicknesses > 50 mm, whilst 3.3 mm cells may be used in components with void thicknesses < 10 mm.

The TPMS equations [20] define a mathematical surface with zero thickness. To create a sample with volume, the surface is 'thickened' to provide a proportion of solid material per volume, termed the 'volume fraction'. In this study, 0.2 and 0.5 vol fraction variants were manufactured for each unit-cell type and cell number combination. This represents the typical range of volume fractions at which lattice structures are used as below 0.2 vol fraction at 3.3 mm cell size, the features become too small to manufacture via LPBF; greater than 0.5 vol fraction, lattice structures lose value as a method of lightweighting and the drawbacks of the increased design complexity outweigh the performance benefits.

Pure thermal conductivity is governed by the volume fraction, i.e. the amount of material available to enable heat transfer. However, it is expected that thermal conductivity will also be a function of geometry in complex structures such as the TPMS lattice types, this constituting a second order effect that must be understood for lattice implementation in components. A combination of parameters was chosen to investigate

Table 1

Parameters used for the manufacture of a total of 18 lattice test samples.

Unit-cell type	Gyroid; Diamond; Schwarz P
Volume fraction	0.2; 0.5
Cell size (mm)	0.33; 5; 10

the effect of the lattice type and XYZ dimensions on the thermal conductivity of the sample, as well as to check the relative weighting of these effects in comparison to the volume fraction.

Initial results from this range of samples were used to generate design equations that allow samples with custom thermal conductivity to be manufactured. These equations take into account the effect that each lattice geometry has on its thermal conductivity, allowing calculation of the required volume fraction. This technique was used to manufacture three further samples of each material, one of each unit cell type, with the target thermal conductivity values of 3.0, 3.5 and $4.0 \text{ W.m}^{-1}. \text{K}^{-1}$ and 1.75, 2.0 and $2.5 \text{ W.m}^{-1}. \text{K}^{-1}$ for Hastelloy-X and Ti6Al4V respectively. The experimentally measured performance of these designed lattices were compared with the predicted performance.

The developed design equations were then used to propose some graded lattice structures in both 2-D and 3-D, with example cases given for each. To demonstrate the design concept visually, a sample with the University of Nottingham logo displayed in graded lattice was manufactured in Hastelloy-X, with the aim of producing a distinct thermal profile when viewed with a thermal camera.

2.3. Materials and manufacturing

Specimens were built in two material types. Hastelloy-X feedstock material was supplied by Oerlikon Metco (MetcoAdd HX-A) and the Ti-6Al-4 V feedstock was supplied by LPW Technology (LPW Ti64 Gd23). All samples were manufactured using a Realizer SLM 50 LPBF machine with the process parameters given in Table 2. These parameters are a reduced laser power version of the standard process parameters used on this system to prevent excessive energy input for fine featured geometries such as lattice structures.

After manufacture, the samples were removed from the build plate using a SiC abrasive cut-off disk and ground flat to within ± 0.05 mm of the nominal $20 \times 20 \times 20$ mm sample dimensions using SiC grinding paper. A final grinding step using P1200 SiC was undertaken to enhance thermal coupling and hence heat transfer. All samples were ultrasonically cleaned to remove loose powder, thoroughly dried and then measured and weighed for calculation of true volume fraction.

2.4. Conductivity apparatus

The test rig used for the experiments was built to conform with ASTM E1225-13 for measurement of the thermal conductivity of a sample using the comparative-longitudinal heat flow technique [21]. A schematic layout of the apparatus is given in Fig. 2. The test stack is comprised of a lattice sample, the specimen, placed between two reference blocks of AISI 304 stainless steel (thermal conductivity, $\lambda_M = 16.2 \text{ W.m}^{-1}. \text{K}^{-1}$ at 293 K) under 5 kg of axial load. Silver sheets (0.5 mm) with two metallurgically bonded T-type thermocouples were placed at every interface as shown in Fig. 2(b). A thin layer of thermal grease was applied between each interface to ensure good thermal coupling. The bottom side of the test stack was heated by a PID regulated PTC element to a constant 443 ± 0.5 K, and the top side was cooled to 295 ± 1.0 K using a water-cooled copper heatsink. The aluminium guard cylinder surrounding the test stack was heated to the mean temperature between the hot and cold sides of the stack, 369 ± 1.0 K. A fibre blanket ($\lambda = 0.04 \text{ W.m}^{-1}. \text{K}^{-1}$ at 473 K) was placed between the test stack and the guard cylinder for thermal isolation and to prevent convective heat transfer currents establishing around the test stack.

After assembling the test stack, heating was undertaken, and the test rig was left for a minimum of 60 min to reach steady state (< 0.1 K/min drift from the prescribed temperatures). The temperatures at each reference block and sample interface were logged using a Pico TC-08 (Pico Technology, UK) thermocouple data logger at 1 s intervals and stored on a PC.

Table 2

Process parameters used to manufacture the lattice samples on the Realizer SLM 50 LPBF machine.

Material	Laser Power (W)	Point Distance (μm)	Exposure Time (μs)	Hatch Distance (μm)	Layer Thickness (μm)	Hatch Scan
Ti6Al4V	82.5	30	40	90	40	1*X, 1*Y
Hastelloy-X	100	10	12	90	40	67 ° Rot

2.5. Calculation of thermal conductivity

The thermal conductivity of the lattice samples was calculated from the temperature gradients set up in the test stack. As the thermal conductivity of the reference blocks is known, it is possible to calculate the thermal conductivity of the sample (λ_s) from the temperature drop across the sample and reference blocks at steady state, using the following equation taken from ASTM E1225-13 [21]:

$$\lambda_s = \frac{Z_4 - Z_3}{T_{UM} - T_{LM}} \frac{\lambda_M}{2} \left(\frac{T_{LM} - T_B}{Z_2 - Z_1} + \frac{T_T - T_{UM}}{Z_6 - Z_5} \right)$$

The nomenclature used in this equation can be drawn from Fig. 2(b). The contribution of the silver sheets to the temperature drop across the stack is assumed to be negligible due to the relatively high thermal conductivity of silver ($\lambda = 420 \text{ W.m}^{-1}.K^{-1}$ at 293 K). This is between 40–60 times the thermal conductivity of the base alloys used to manufacture the specimens in this experiment. It should be noted here that this standard and the calculation above generally relates to conduction in a solid material. In our case we have a geometric structure consisting of air and metal. Whilst the high conductivity of the metal would indicate that this would be the main heat flow path in the test, it should be noted that heat flow is also possible through conduction and convection in the air. Another factor with the lattice geometry is that it will affect the heat flow path in the metal. For this reason the test should be considered as measuring an ‘apparent conductivity’ that is a measure of both material and geometry rather than a pure material property.

2.6. Uncertainty analysis

For this experiment, errors that arise from heat exchange between the test stack and the guard, and heat shunting through the insulation surrounding the test stack, were assumed to be negligible. This assumption was tested by altering the temperature of the guard cylinder from room temperature (~294 K) to 373 K, noting that minimal change of measured conductivity for the test specimen was measured.

For error calculation, the following values were used - maximum uncertainty in thermocouple temperature reading: 0.2% of the reading + 0.5 K; uncertainty in the thermal conductivity of the reference blocks: 5%. Indeterminate errors caused by heat exchange between stack and surroundings, heat shunting through insulation, non-uniform interfacial resistance and random uncertainty were minimised by repeating experiments, and were evaluated to be less than 3% of the measured value. Therefore, the uncertainty in the measurement of the thermal conductivity of the samples using this method was determined to be a maximum of $\pm 7.0\%$ for the Hastelloy-X and Ti6Al4V samples.

3. Results and discussion

3.1. Thermal conductivity testing

Fig. 3 shows the apparent thermal conductivity measured from the experiments as a function of actual volume fraction (volume fraction as measured from manufactured samples) and lattice cell type for the two different metal alloys. It can be seen that there is a linear relationship between the volume fraction and the thermal conductivity for all lattice types within the volume fraction range tested, in both Hastelloy-X and

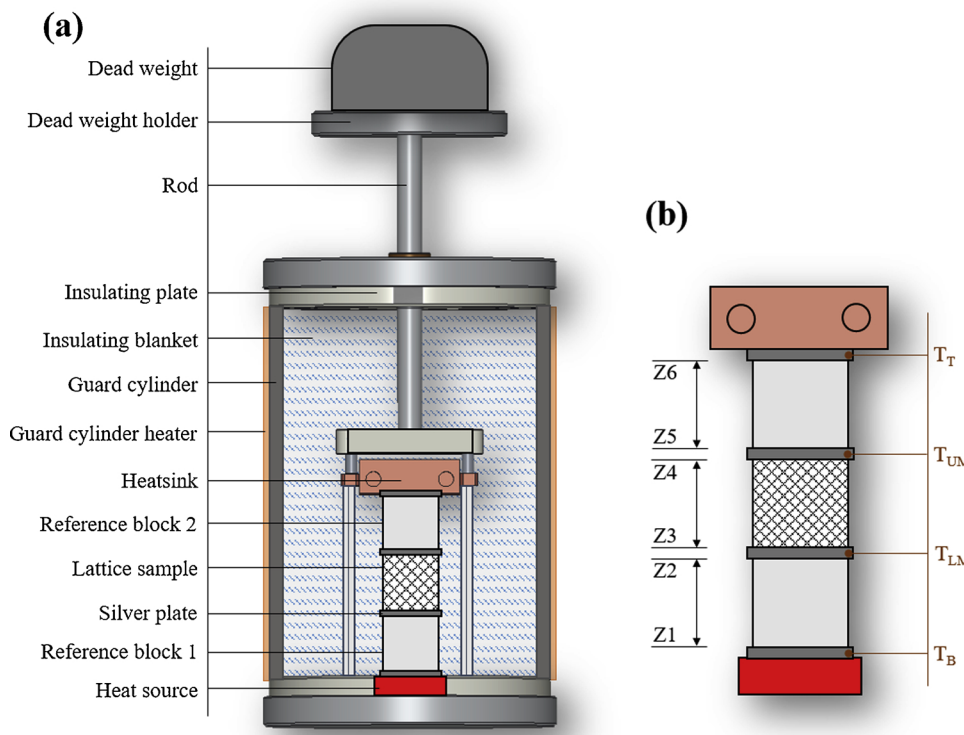


Fig. 2. (a) Schematic of the thermal conductivity testing apparatus used to measure the thermal conductivity of the lattice samples using the ASTM E1225-13 comparative-longitudinal heat flow technique. (b) Enlarged view of the test stack indicating the position of the measurements taken for the calculation of apparent thermal conductivity of the sample.

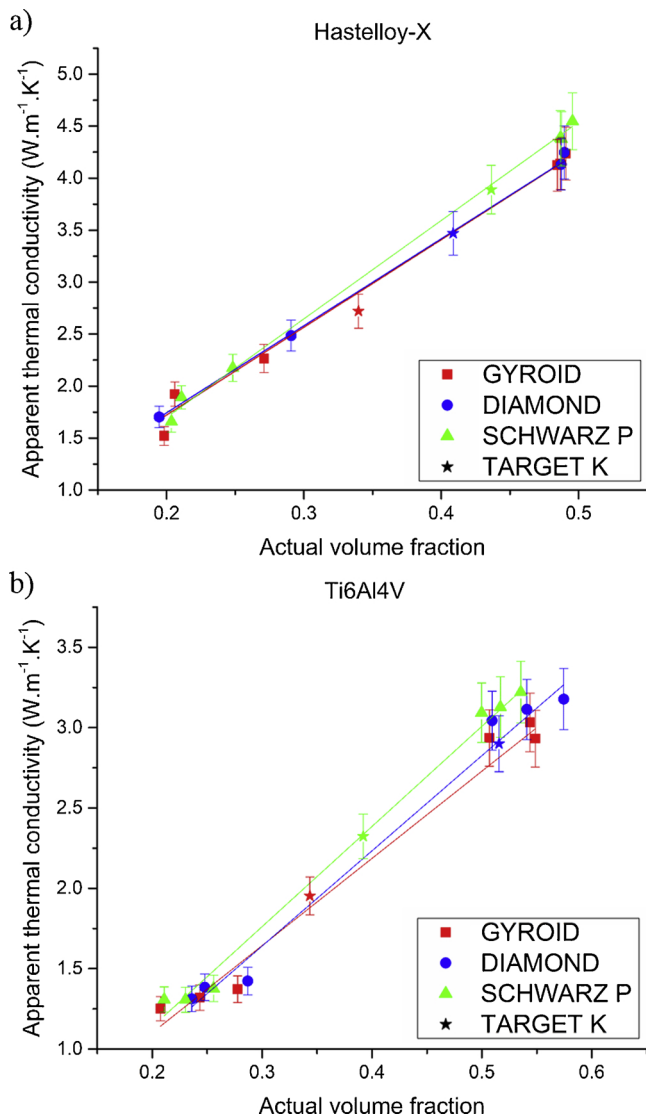


Fig. 3. Apparent thermal conductivity against actual volume fraction for all Hastelloy-X (a) and Ti6Al4V (b) lattices. The unit cell type is denoted, but the cell size is ignored for this plot. The star markers are the results of the ‘specified conductivity’ test, where new lattices with specific conductivity were manufactured from the equations of the lines of best fit shown above. Error bars consistent with 7% (see 2.6).

Ti6Al4V. This is regardless of the unit cell size. The diamond and gyroid unit cells perform similarly for both materials, whilst the Schwarz primitive unit cell has a slightly higher thermal conductivity per volume fraction. Whilst the measurement variation is relatively large for these results, the pattern is closely matched in both materials tested. This effect is attributed to the increase in wall thickness (or decrease in surface area to volume ratio, as evidenced in Table 3) seen in this unit cell compared to the gyroid and diamond unit cells. This has the effect of providing fewer but wider conduction pathways for the heat, with a lower proportion of heat energy lost due to radiation and conduction into the air contained within the unit cell. Further, the thicker wall provides better thermal contact between the lattice sample and the reference blocks when assembled in the test stack.

The data in Fig. 3 was fit to an equation of the form

$$K_a = C_1 V_f + C_2 \quad (1)$$

Where K_a is apparent thermal conductivity, V_f is volume fraction and C_i are the fitting constants relating to a particular lattice cell type and material. The curve fit constants are provided in

Table 3

Surface area and volume data for each lattice sample tested based upon the computer models. Note the large variation in surface area to volume ratio between the unit cell types, giving rise to the differences in conductivity seen in Fig. 3.

Unit cell	Vol. frac.	Cell size (mm)	Surface area (mm ²)	Volume (mm ³)	SA : vol	Min. wall thickness (μm)
GYROID	0.2	3.33	14960	1572	9.52	230
	0.2	5	10128	1591	6.37	355
	0.2	10	5252	1584	3.31	695
	0.5	3.33	14109	3994	3.53	610
	0.5	5	9790	3986	2.46	910
DIAMOND	0.5	10	5429	4008	1.35	1820
	0.2	3.33	18583	1509	12.31	190
	0.2	5	12485	1584	7.88	275
	0.2	10	6412	1584	4.05	555
	0.5	3.33	17131	4004	4.28	490
SCHWARZ P	0.5	5	11793	3995	2.95	730
	0.5	10	6379	4006	1.59	1480
	0.2	3.33	11399	1595	7.15	265
	0.2	5	7744	1590	4.87	400
	0.2	10	4050	1590	2.55	795
TARGET K	0.5	3.33	10584	4005	2.64	685
	0.5	5	7406	3999	1.85	1030
	0.5	10	4210	4000	1.05	2070

Table 4

Curve fitting parameters for the linear equations relating apparent thermal conductivity to actual volume fraction for each of the unit cell types.

		C_1	C_2
H-X	GYR	8.631	-0.039
	SCH	9.415	-0.174
	DIA	8.507	+0.032
Ti6Al4V	GYR	0.056	-0.024
	SCH	0.063	-0.129
	DIA	0.060	-0.149

Table 4. To validate this linear fit, some samples with a specified thermal conductivity were manufactured and tested. The samples were varied in unit cell and cell size, and the required volume fraction was calculated from Eq. (1) using the constants in Table 4. A description of the samples manufactured in this exercise and the corresponding geometrical data is given in

Table 5. The data from the samples manufactured to have a specified thermal conductivity were also added to Fig. 3 (star data points); it is clear that there is a good correlation between these samples and the linear fit from which the volume fractions are calculated. This gives confidence that the design equations can be used to manufacture lattice structures with a specific thermal conductivity. However, the target conductivity experiment highlighted the discrepancy between the designed volume fraction and the actual (manufactured) volume fraction, where in each case the Ti6Al4V samples had 5.1–9.5 % higher volume fraction than designed (

Table 5. ‘Vol. frac. % diff.’). This resulted in higher thermal conductivity values than expected, with the deviation range of 10.3–13.8 % being outside of the 7% maximum standard error of the system. The Hastelloy-X samples had higher volume fraction accuracy with a deviation from designed value of -3.0 – 0.8%, with correspondingly more accurate thermal conductivity results, with the diamond 10 mm cell sample coming within 1% of the designed value. This relationship between designed volume fraction and actual volume fraction after manufacture is dependent upon geometry, material and process parameters. It is a further optimisation parameter that needs to be taken into account when designing lattice structures for a specified load, whether the load is mechanical or thermal. There is no simple correction that can be applied to all TPMS lattices to achieve 100% accuracy to the. stl

Table 5

Design parameters and experimental test data for the three target thermal conductivity lattice samples manufactured in each material.

Unit cell	Cell size (mm)	Target cond. ($\text{W} \cdot \text{m}^{-1} \cdot \text{K}^{-1}$)	Designed vol. frac.	Actual vol. frac.	App. cond. ($\text{W} \cdot \text{m}^{-1} \cdot \text{K}^{-1}$)	Vol. frac. % diff.	Cond. % diff.
Hastelloy-X							
GYR	3.33	3.00	0.350	0.340	2.72	-3.0	-10.4
SCH	5	4.00	0.440	0.436	3.89	-0.8	-2.7
DIA	10	3.50	0.415	0.409	3.47	-1.6	-0.7
Ti6Al4V							
GYR	3.33	2.50	0.467	0.516	2.90	9.5	13.8
SCH	5	2.00	0.372	0.392	2.32	5.1	13.8
DIA	10	1.75	0.325	0.343	1.95	5.2	10.3

model; corrections must be developed on a case-by-case basis. These corrections may be made directly to the .stl file, such as applying a scaling factor, or to the processing parameters to ensure the manufactured part is accurate to the digital model.

Design rules such as the linear fit developed here are vital for components where a load bearing wall may also be required to provide a thermally insulating layer by using lattice structures in a sandwich construction. If there is no coolant fluid passing through this layer, thermal conductivity dominates and hence it must be possible to accurately control the thermal conductivity of the structure used. Alternatively, such lattice structures can be used as a heatsink to conduct heat away from high-temperature components. Whilst the materials shown in this paper may not be ideal for high-performance conductive heat transfer, they are commonly preferred for gas turbine applications. This is an application where materials with a higher thermal conductivity, aluminium or copper alloys, cannot provide adequate performance at the high operating temperatures.

To aid analysis of unit cell type and size, the parameter ‘normalised conductivity’ was used. This was calculated by dividing the thermal conductivity by the actual volume fraction for each sample. This removes the effect of the volume fraction from the data set and hence allows for any cell size effect to be studied. The results were sorted by material and grouped by designed volume fraction, as presented in Fig. 4. It can be seen that the Schwarz primitive lattice samples had a greater conductivity than gyroid or diamond based samples of the same cell size and volume fraction in 92% of the applicable test cases, mirroring the results from Fig. 3. This is independent of material and is attributed to the lower surface area to volume ratio seen in the Schwarz primitive cell type.

The relationship between lattice sample and the thermal conductivity is dominated by the volume fraction. However, if this was the only factor in the relationship, then for each material in Fig. 4 the value of normalised conductivity would be equal across all cell sizes. However, it can be seen that the normalised conductivity changes across the 0.2 vol fraction samples for both materials; at 3.33 mm cell size, the normalised conductivity is typically 8–20 % lower than for the same unit cell type at 10 mm cell size. At small cell sizes, the wall thicknesses are significantly lower than for larger cell sizes at the same volume fraction. This geometrical relationship is clear when considering a cross-sectional area of a particular unit cell across a range of unit cell sizes whilst keeping the volume fraction equal, as seen in Fig. 5. A reduced wall thickness results in a decreased heat transfer efficiency and an increased probability of poor thermal coupling between the lattice sample and the reference blocks. Further, surface roughness of LPBF components remains relatively constant across all wall thicknesses (for each build angle relative to the build plane). For thin walls, surface roughness occupies a greater proportion of the total wall thickness than for thicker walls. Surface roughness consists of partially fused powder particles that will have limited thermal transport ability due to a lack of metallurgical bond or physical contact, effectively reducing the thermal conductivity. Therefore, geometries with a lower average wall thickness may show reduced thermal conductivity. These effects act to decrease the apparent thermal conductivity of the sample.

Throughout this experiment, the contribution of convective heat transfer between cells was assumed to be negligible. This is true for the smaller cell sizes, where the tightly spaced cells prevent air currents from moving large distances in the z-direction; at larger cell sizes, the path for convection is wider and so convection between the cells may increase the apparent thermal conductivity of the samples. Thermal conductivity measurement error due to natural convection is discussed in ASTM E1225-13 [21] with regards to heat flow external to solid samples. Whilst this standard does not deal with porous samples, the principles of measurement error due to natural convection can be applied to the lattice samples. This is seen particularly in the 0.2 vol fraction samples, Fig. 4(a) and (c). At 0.5 vol fraction, the increase in material reduces the free volume inside each cell and constricts the pathways for convection between cells. Hence, this is why an increased cell size does not have as great an impact on the thermal conductivity for these samples (Fig. 4(b) and (d)). As such, if it is desirable to design a lattice that acts as a natural convection heatsink, it is important to ensure a cell size and volume fraction is chosen that allows for sufficient convection between cells and hence flow of fluid out of the heatsink structure.

3.2. Development of samples with graded thermal conductivity

The design equations previously provided were fed back into the lattice design software to create sample models with prescribed variations in thermal conductivity. As the TPMS lattices shown here are not based on nodes and elements, but instead are mathematically represented surfaces, the volume fraction can be continuously varied in 3-dimensions. This avoids the step change in volume fraction and hence thermal conductivity that would be seen if a discrete cell-by-cell variation was used. Fig. 6(a) illustrates a simple 1D variation in volume fraction, and hence apparent thermal conductivity, in the z-direction of the sample based on a shallow gradient parabolic function. The range of $1.875\text{--}4.5 \text{ W} \cdot \text{m}^{-1} \cdot \text{K}^{-1}$ in Hastelloy-X corresponds to 0.22–0.5 vol fraction and hence covers the majority of the volume fraction range tested experimentally. The effect of volume fraction on wall thickness is clearly seen by observing the expansion and contraction of the hole in the side wall of the Schwarz primitive unit cell type used in this sample. Fig. 6(b) introduces further complexity into the grading by using a cosine squared function.

Similar design methods can be applied to generate a sample that has a 2D graded structure. Fig. 7 illustrates a gradient based upon a 2D function, creating a sinusoidal variation in volume fraction, and hence thermal conductivity, that resonates out from the centre of the sample. Such a structure could be placed on top of a flat plate heater, with the heat being conducted through the lattice structure. Therefore, a heating device with a very specific heat distribution can be produced without requiring a custom resistive element or filament to be manufactured. Designing a conventional heating element that can vary the temperature profile with sub millimetre-scale precision is trivial to produce using graded lattice structures via LPBF.

Using this method of varying volume fraction, a custom lattice was designed that included the University of Nottingham castle logo and ‘UoN’ text. The .stl model and manufactured sample, the latter coated in

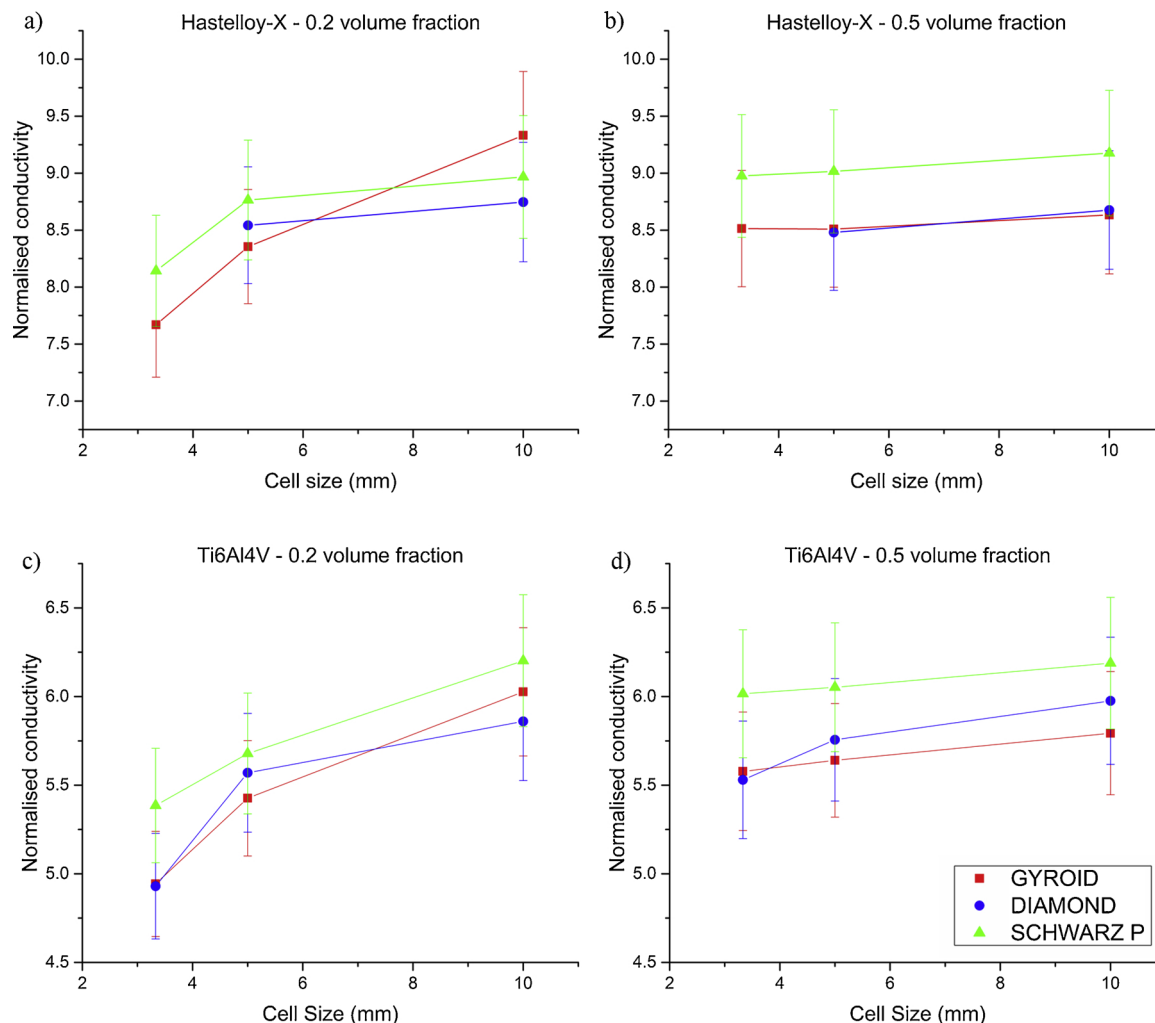


Fig. 4. Normalised conductivity vs cell size for Hastelloy-X (top row) and Ti6Al4V (bottom row) lattice samples with 0.2 vol fraction (a), (c) and 0.5 vol fraction (b), (d). Using normalised conductivity (apparent conductivity / volume fraction) allows for the effect of unit cell type and cell size to be analysed independently to the effect of volume fraction.

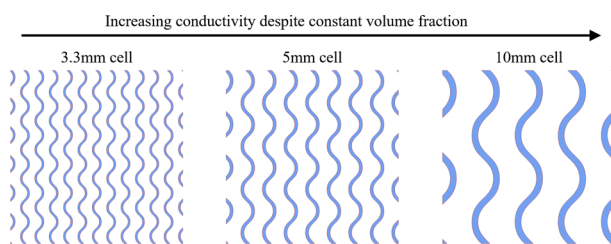


Fig. 5. An illustration of the change in wall thickness across different unit cell sizes despite a constant volume fraction (0.2 in this case). This has an effect on the apparent conductivity of the lattice that is independent of the volume fraction. However, in manufactured samples, some variation may also be due to surface roughness occupying a larger proportion of the solid material in thin walls, leading to decreased thermal conductivity.

matt black paint to aid in capturing a thermal image, can be seen in Fig. 8. This custom lattice sample was then placed on a heater plate and a FLIR T400 infrared camera was used to capture images as the plate heated up. Despite appearing as a near-uniform lattice sample to the naked eye, the logo and text can be distinguished from the background using the infrared imaging method (Fig. 8c). The high resolution and sharp definition between the logo and the background was achieved due to the continuous cell grading. This image was captured before the temperature of the sample reached steady state; the lower temperature

seen in the logo region is a consequence of the higher thermal mass of this area due to the higher volume fraction. At steady state, the temperature profile would be uniform across the sample. If this sample was to be used as an interface between the heater plate and a component, heat would be conducted at a higher rate through the logo and text area (higher volume fraction areas) than the surrounding lattice.

4. Conclusions

In this study, the apparent 1D thermal conductivity for a range of lattice samples was experimentally derived using a custom-built test rig conforming to ASTM E1225-13. The derived results were then used to develop a set of design rules, or equations, that govern the relationship between thermal conductivity and the lattice parameters of volume fraction, unit cell type and unit cell size. From these design rules, it was possible to generate a number of demonstration models with a prescribed variation in conductivity using 1D and 2D mathematical functions. A sample was manufactured using the University of Nottingham logo to demonstrate how varying the lattice volume fraction results in a distinct thermal profile. As a result of this work, heatsinks or thermal insulation layers can be developed that are optimised for thermal conductivity whilst retaining the advantages in weight reduction that lattice structures provide. Example applications across electronics, automotive and aerospace industries are given in the results and discussion section.

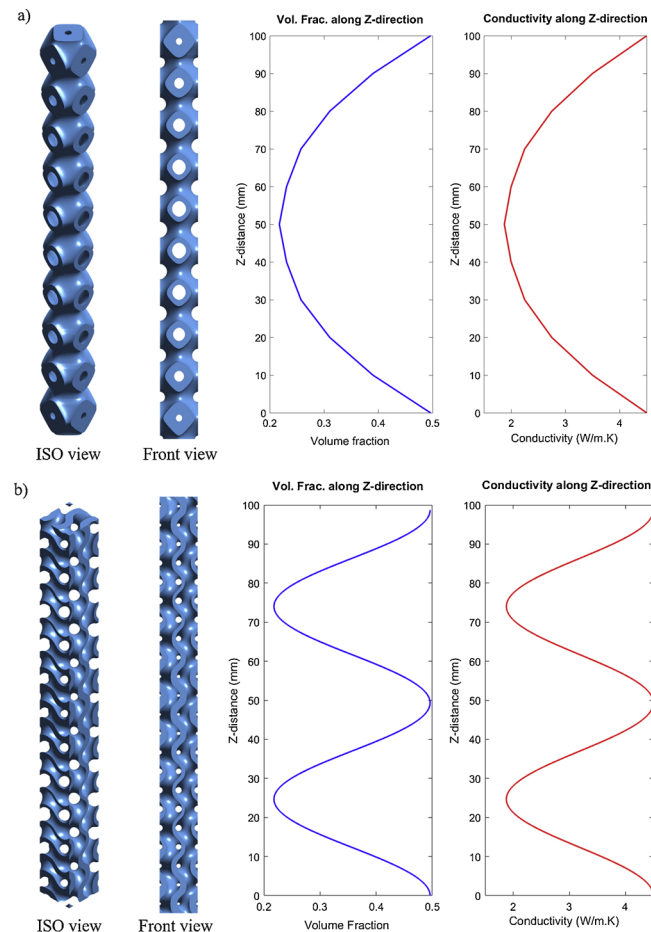


Fig. 6. Demonstration of 1D functional grading of Hastelloy-X lattice structures to sweep through a prescribed range of apparent thermal conductivities through variation of volume fraction following (a) a simple gradient and (b) a cosine squared gradient. This functional grading is based upon the design rules developed from the experimental data.

The key findings of the study are as follows:

- For the lattice structures tested, thermal conductivity is primarily a function of the volume fraction, or ratio of solid material to free

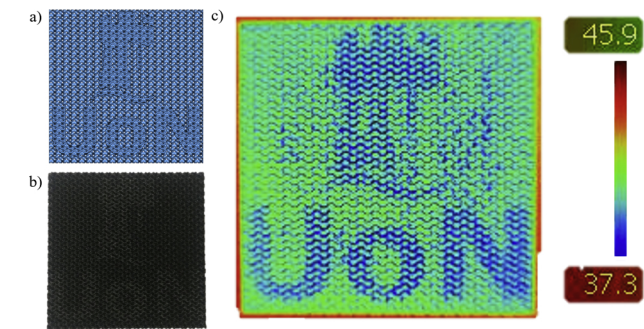


Fig. 8. University of Nottingham logo and text embedded into a lattice sample using variation in volume fraction. The stl file can be seen in a) along with the manufactured sample in b) after spraying matt black. The logo is barely visible to the naked eye until it is heated and the variation in temperature due to the volume fraction grading is captured with an infrared camera, c). Temperatures shown in °C.

space inside the lattice

- Unit cell types with higher minimum wall thickness have a greater thermal conductivity than those with lower minimum wall thickness, at the same volume fraction (i.e. thermal conductivity is inversely proportional to surface area to volume ratio). It is important to note that for convective heat transfer, thermal performance is typically proportional to surface area, so thin walls are likely to be more beneficial under convection.
- Surface roughness may have a greater effect on thermal conductivity for samples with a higher surface area to volume ratio. Partially fused material at the surface has reduced thermal conductivity, therefore the material will not be as efficiently distributed within a sample with more surface area.
- Smaller unit cell sizes may constrain the air within the cells, preventing natural convection heat transfer between the cells from increasing the measured thermal conductivity.
- Larger unit cells may allow air to flow freely between cells, increasing the measured thermal conductivity. This effect is greater for unit cell types with a lower surface area to volume ratio such as Schwarz primitive

Typically, heatsinks used to cool electronics or mechanical components are independent components or assemblies. This creates complexity in manufacture and assembly, where components are joined using mechanical methods. Further, the packing of components is not

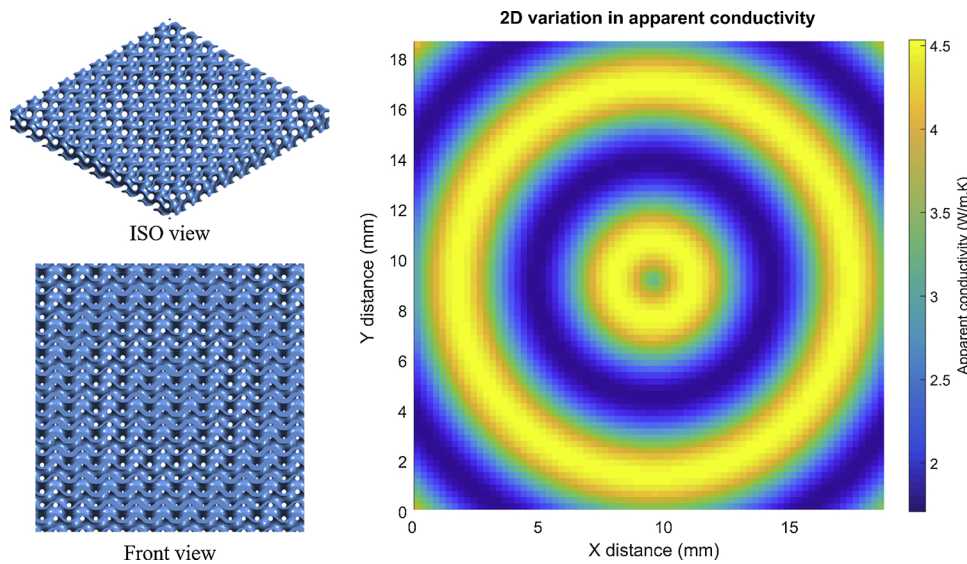


Fig. 7. A demonstration of 2D functional grading of Hastelloy-X lattice structures based upon the $\sin(x^2 + y^2)^{-1}$ function, showing prescribed apparent thermal conductivity within the range 1.875–4.5 W/(m.K). On the left is the digital model of the lattice structure generated with the 2D volume fraction map shown on the right.

optimised. This is a particular issue in aerospace and automotive components, where both volume and mass are at a premium. But most importantly, the weight of the assembly is increased by the necessity of manufacturing each component separately. Through simulation of the thermal loads, a thermal profile for the components can be derived. From this, a custom heatsink can be incorporated into the component itself. This design can be optimised for: minimal weight; defined thermal properties to cool hot components; structural strength (if load bearing) or external volume and shape for efficient packaging. In more advanced lattice applications, a coolant flow such as compressed air can be forced through the structure. Operating as heat transfer surfaces under forced convection, lattice structures are capable of adding value to components in multiple ways. With proper design knowledge, such features can be incorporated into components via LPBF without incurring significant material cost or manufacturing time penalties. Therefore, the experimental study of lattice structures as convective heat transfer devices is the next research challenge.

Acknowledgments

This work was funded through the EPSRC (Engineering and Physical Sciences Research Council, UK)Centre for Doctoral Training in Additive Manufacturing and 3D Printing [EP/L01534X/1], Industrial Cooperative Awards in Science & Technology (CASE) [16000180], Siemens Industrial Turbomachinery Ltd, Lincoln, UK and Leonardo S.p.A. The authors would like to acknowledge and thank Mr Alex Jackson-Crisp for his technical assistance in the manufacture of the testing apparatus.

References

- [1] C. Yap, et al., Review of selective laser melting: materials and applications, *Appl. Phys. Rev.* 2 (4) (2015) 041101.
- [2] A. du Plessis, et al., Beautiful and functional: a review of biomimetic design in additive manufacturing, *Addit. Manuf.* 27 (2019) 408–427.
- [3] D. Bhate, et al., Classification and selection of cellular materials in mechanical design: engineering and biomimetic approaches, *Designs* 3 (1) (2019) 19.
- [4] A. Panesar, et al., Strategies for functionally graded lattice structures derived using topology optimisation for additive manufacturing, *Addit. Manuf.* 19 (2018) 81–94.
- [5] R.K. Shah, D.P. Sekulic, *Fundamentals of Heat Exchanger Design*, John Wiley & Sons, 2003.
- [6] K. Thulukkanam, *Heat Exchanger Design Handbook*, CRC Press, 2013.
- [7] C. Marques, K.W. Kelly, Fabrication and performance of a pin fin Micro heat exchanger, *J. Heat Transf.* 126 (3) (2004) 434–444.
- [8] J.-J. Hwang, C.-C. Lui, Measurement of endwall heat transfer and pressure drop in a pin-fin wedge duct, *Int. J. Heat Mass Transf.* 45 (4) (2002) 877–889.
- [9] T. Wen, et al., Forced convection in metallic honeycomb structures, *Int. J. Heat Mass Transf.* 49 (19) (2006) 3313–3324.
- [10] T.J. Lu, Heat transfer efficiency of metal honeycombs, *Int. J. Heat Mass Transf.* 42 (11) (1999) 2031–2040.
- [11] J.H. Joo, et al., Forced convective heat transfer in all metallic wire-woven bulk Kagome sandwich panels, *Int. J. Heat Mass Transf.* 54 (25–26) (2011) 5658–5662.
- [12] D.T. Queheillalt, et al., A multifunctional heat pipe sandwich panel structure, *Int. J. Heat Mass Transf.* 51 (1–2) (2008) 312–326.
- [13] I. Maskery, et al., Mechanical properties of Ti-6Al-4V selectively laser melted parts with body-centred-Cubic lattices of varying cell size, *Exp. Mech.* 55 (7) (2015) 1261–1272.
- [14] M. Smith, Z. Guan, W.J. Cantwell, Finite element modelling of the compressive response of lattice structures manufactured using the selective laser melting technique, *Int. J. Mech. Sci.* 67 (2013) 28–41.
- [15] T. Kim, H. Hodson, T. Lu, *Pressure loss and heat transfer mechanisms in a lattice-frame structured heat exchanger*, *Proc. Inst. Mech. Eng. Part C J. Mech. Eng. Sci.* 218 (11) (2004) 1321–1336.
- [16] T. Kim, et al., Convective heat dissipation with lattice-frame materials, *Mech. Mater.* 36 (8) (2004) 767–780.
- [17] S. Gu, T.J. Lu, A.G. Evans, On the design of two-dimensional cellular metals for combined heat dissipation and structural load capacity, *Int. J. Heat Mass Transf.* 44 (11) (2001) 2163–2175.
- [18] M. Wong, et al., Selective laser melting of heat transfer devices, *Rapid Prototyp. J.* 13 (5) (2007) 291–297.
- [19] M. Wong, et al., Convective heat transfer and pressure losses across novel heat sinks fabricated by Selective Laser Melting, *Int. J. Heat Mass Transf.* 52 (1–2) (2009) 281–288.
- [20] J. Shi, et al., A TPMS-based method for modeling porous scaffolds for bionic bone tissue engineering, *Sci. Rep.* 8 (1) (2018) 7395.
- [21] Standard Test Method for Thermal Conductivity of Solids Using the Guarded-Comparative-Longitudinal Heat Flow Technique, ASTM International, 2013.